

Circumstellar and Circumbinary Disks in Eccentric Stellar Binaries

Barbara Pichardo^{1,2*}, Linda S. Sparke^{1*}, Luis A. Aguilar^{3*}

¹*Department of Astronomy, 475 North Charter Street, University of Wisconsin-Madison, Madison WI 53706-1582, USA*

²*Department of Physics and Astronomy, University of Kentucky, Lexington, KY 40506-0055, USA*

³*Observatorio Astronómico Nacional, IAUNAM Ensenada, Apdo. postal 877, 22800 Ensenada, México*

Accepted . Received ; in original form

ABSTRACT

We explore test particle orbits in the orbital plane of eccentric stellar binary systems, searching for “invariant loops”: closed curves that change shape periodically as a function of binary orbital phase as the test particles in them move under the stars’ gravity. Stable invariant loops play the same role in this periodically-varying potential as stable periodic orbits do in stationary potentials; in particular, when dissipation is weak, gas will most likely follow the non-intersecting loops, while nearby particle orbits librate around them. We use this method to set bounds on the sizes of disks around the stars, and on the gap between those and the inner edge of a possible circumbinary disk. Gas dynamics may impose further restrictions, but our study sets upper bounds for the size of circumstellar disks, and a lower bound for the inner radius of a circumbinary disk. We find that circumstellar disks are sharply reduced as the binary’s eccentricity grows. For the disk around the secondary star, the tidal (Jacobi) radius calculated for circular orbits at the periastron radius, gives a good estimate of the maximum size. Disks change in size and shape only marginally with the binary phase, with no strong preference to increase or decrease at any particular phase. The circumstellar disks in particular can be quite asymmetric. We compare our results with other numerical and theoretical results and with observations of the α Centauri and L1551 systems, finding very good agreement. The calculated changes in the shapes and crowding of the circumstellar orbits can be used to predict how the disk luminosity and mass inflow should vary with binary phase.

Key words: circumstellar matter, disks – binary: stars.

1 INTRODUCTION

Most low-mass main-sequence stars are members of binary or multiple systems (Duquennoy & Mayor 1991, Fischer & Marcy 1992). The binary frequency of pre-main-sequence stars is also high, and probably higher than for main-sequence stars (Mathieu, Walter & Myers 1989; Simon et al. 1992; Ghez, Neugebauer & Matthews 1993; Leinert 1993; Reipurth & Zinnecker 1993). In the last decade, interest in these systems has increased significantly with the discovery that many T-Tauri and other pre-main-sequence binary stars, possess both circumstellar and circumbinary disks (for a review see Mathieu 1994). Observations of binary systems suggest the existence of disk material around one or both stars, as is inferred from observations of excess radiation at infrared to millimeter wavelengths, polarization, and both

Balmer and forbidden emission lines (Mathieu 2000). Some extrasolar planets have been found to orbit stars that have a stellar companion, e.g., 16 Cygni B, τ Bootis, and 55 ρ Cancri (Butler et al. 1997; Cochran et al. 1997), confirming that planets can form in binary star systems. Thus the study of stellar disks in binary systems, as well as the possibility of stable orbits, is a key element for better understanding stellar and planetary formation.

It is currently believed that multiple stellar systems result from fragmentation, which produces mainly eccentric binaries (Bonnell & Bastien 1992, Bate 1997; Bate & Bonnell 1997), in particular wide stellar systems with separations ≥ 10 AU (Bate, Bonnell & Bromm 2002). Although main-sequence binary systems typically have eccentric orbits (Duquennoy & Mayor 1991), most theoretical studies have focused on binaries in near-circular orbits. Extensive and very good theoretical work has been done here (Lubow & Shu 1975; Paczyński 1977; Rudak & Paczyński 1981; Pa-

* E-mail: barbara@pa.uky.edu (BP); sparke@astro.wisc.edu (LSS); aguilar@astrosen.unam.mx (LAA)

paloizou & Pringle 1977; Bonnell & Bastien 1992, Bate 1997; Bate & Bonnell 1997).

Only a few observed pre-main sequence binaries have known orbital elements (Pogodin et al. 2004; Schaefer et al. 2003; Masciadri & Raga 2002) and information on the accompanying disks is even rarer (Kastner 2004; Jensen et al. 2004; Nielbock 2003; Liu 2003; Rodriguez et al. 1998, and references therein). From the observational point of view, measuring the size of a circumstellar disk is quite difficult, since these are typically $< 100 AU$ across. Modelers also have a hard task, since dynamical effects like resonances can introduce very fine and complicated structure. In circular binaries, where the gravitational potential is fixed in a uniformly-rotating frame, and an energy-like integral is conserved along particle orbits, the position and strength of resonances can be calculated. In the interesting eccentric case, we lack a conserved integral, and it is not clear how to proceed. One of the most important studies to date is by Artymowicz & Lubow (1994), who compute analytically the position of orbital resonances (between 1:4 and 1:3) in the circumstellar disks, and approximate the sizes of disks by computing the radius where resonant and viscous torques balance each other. Their results, however, depend strongly on the badly-constrained viscosity parameter.

The complexity of the problem has prompted some researchers to use direct 3-body simulations to study the possible existence of stable orbits for planets around eccentric orbits (David et al. 2003 and references therein). This approach, however, is computationally expensive when accuracy is required. Others have used hydrodynamic simulations (Foulkes et al. 2004; Guerrero, García-Berro, Isern 2004; Lanzafame 2003 and references therein). Unfortunately these simulations depend sensitively on the unknown viscosity as well, and are quite expensive computationally.

In this work we have opted for a simpler approach, analogous to using the structure of periodic orbits in a circular binary, to predict the gas flow. The path followed by a gas parcel in a stable disk around a star must not intersect itself, or the path of a neighboring parcel (in the case of planets, the paths may cross and we consider this in the application to a planetary system). Using a test particle method, we probe the orbital structure of binaries of various eccentricities and mass ratios, and identify families of *stable invariant loops*. These consist of closed contours in configuration space, such that as each point initially in them evolves forward in time in the binary potential, the contour changes its shape but comes back to its original form and position when the potential has completed a period (Maciejewski & Sparke 1997, 2000). When invariant loops do not cross, they may be filled with gas; if the gas loses or gains angular momentum it may drift through a sequence of invariant loops.

Although further restrictions may limit the regions occupied by gas in an eccentric binary, our study offers a firm first survey of the regions where gaseous disks and planets cannot exist around stars in eccentric binary systems.

In Section 2.1 we review the concept of an *invariant loop*, and describe our orbit integration method and the strategy used to find invariant loops. The application to the circular binary as a test case is presented in Section 3. The application to the general case of arbitrary orbital eccentricity is shown in Section 4. In Section 6 we apply this study

to observations of L1551 IRS5 and α Centauri. Conclusions are presented in section 7.

2 THE METHOD

2.1 What is an Invariant Loop?

A time-periodic potential in the (two dimensional) orbital plane of an eccentric binary, is mathematically equivalent to a 3-D system with an autonomous Hamiltonian, but with the addition of time (in our case, the binary phase) and the Hamiltonian as two extra dimensions in phase space (e.g. Lichtenberg & Lieberman 1992, Section 1.2). If we restrict ourselves to orbits that lie within the orbital plane of the binary, the extended phase space will have 6 dimensions and regular orbits will lie on a 3-dimensional hypersurface. The motion of a regular orbit is then multiply periodic (Arnold, 1984) with three frequencies, one of which is the oscillation frequency of the potential. If we examine the system at fixed orbital phases, we slice through the extended phase space at a fixed position on the time axis, and the resulting projection of a regular orbit will lie on a 2-dimensional hypersurface, densely filling an area on the orbital plane.

An additional integral of motion would confine an orbit to lie on a 1-dimensional curve. Every time the system comes back to the initial orbital phase, the particle that follows this orbit will land on the same 1-dimensional curve: an *invariant loop*. If we were to “paint” in a series of different colors all particles that initially lie on such a curve, we would see each follow its own path as the binary stars move around each other, distorting the initial shape; but as the binary returns to the initial orbital phase, the painted curve would come back to the same initial locus, and although each particle would be at a different point along the curve, the original order of the colors would be conserved.

Stable invariant loops represent the generalization to periodically time-varying potentials of the stable closed orbits that form the ‘backbone’ of the orbital structure in time-independent potentials. Particle orbits that start near a stable invariant loop will remain trapped close to it, exploring a nearby region in phase space. Gas in a low-viscosity regime trying to settle down in a quasi-static configuration will converge on the non-intersecting stable invariant loops.

2.2 Numerical implementation

We write the equations of motion for the binary star system in term of the eccentric anomaly ψ (e.g. Goldstein 2002, Section 3.7). We use units where the gravitational constant G , the binary semi-major axis a , and its total mass $m_1 + m_2$ are set to unity so that, the binary period is 2π , and its frequency $\omega = 1$. The separation of the two stars at time t , measured from periastron where the azimuthal angle $\theta = 0$, is given by the radius r ,

$$r = a(1 - e \cos \psi), \quad (1)$$

$$\omega t = (\psi - e \sin \psi), \quad (2)$$

$$\cos \theta = a(\cos \psi - e)/r. \quad (3)$$

The binary eccentricity, defined as $e = \sqrt{1 - b^2/a^2}$ where a , and b are the semimajor and semiminor axes, and

the mass ratio $q = m_2/(m_1 + m_2)$ are the only free parameters. We used an Adams integrator (from the NAG fortran library) to follow the motion of a test particle moving in the orbital plane of the two stars. Kepler's equation (1) is solved within a tolerance of 10^{-9} . In the circular case, the Jacobi energy of the test particle (computed as a diagnostic for the quality of the numerical integration) is conserved within one part in 10^9 per binary period.

The equations of motion of the test particle are solved in an inertial reference frame using Cartesian coordinates, with their origin at the center of mass of the binary. All test particle trajectories are launched when the binary is at periastron, with the two components lying on the x -axis. We search initially for families of loops that are symmetric about this line, so we launch test particles at various points along the x -axis and perpendicular to it. We then store the particle's position and velocity every time the stars return to periastron. The computation is halted if the particle runs away, moving further than 10 times the semimajor axis (a) from the center of mass, or if it comes within a distance of either star that results in a high number of force computations, generally due to close approaches to the stars. In this manner, we obtain orbits around each star (circumstellar), orbits around both stars (circumbinary), runaway orbits, and orbits that are captured by one of the stars.

2.3 Searching for Invariant Loops in a Binary System

Among all the possible orbits, we are seeking a very special type: the *invariant loops*, for which the successive phase-space coordinates of our test particle fall on a one-dimensional curve. To find them, we examine the iterates in some two-dimensional subspace, such as the $x - y$ plane. We plot the positions of the test particle at each complete binary period, and compute their dispersion along the radial direction for those that lie within a sector that spans a small angle (5°) about the x axis. Repeating the integration with the same starting x -value, we adjust the launch velocity v_y to minimize this dispersion. In each panel of Figure 1, we show iterates from three particles that orbit around the primary star, and three around the secondary. As v_y is adjusted, the iterates converge towards the loops in panel d.

Effectively, our method finds only stable loops. Particles launched near an unstable loop would rapidly diverge from it, and we would not see the convergence illustrated in Figure 1. Very near the stars, the stable loops are close to stable circular orbits in the potential of that star alone. We exploit this fact to find families of circumstellar loops: we start by launching a particle close to either star, with a speed appropriate to the circular orbit. Once we have found a loop, we move the starting point in small steps away from the star, and use the loops we have just found to predict the next starting speed. The process ends when we can find no more loops with larger starting distances. To map out a family of circumbinary loops, we begin at large radii, where the loops are close to circular orbits about the center of mass; we continue inwards until no more loops are found.

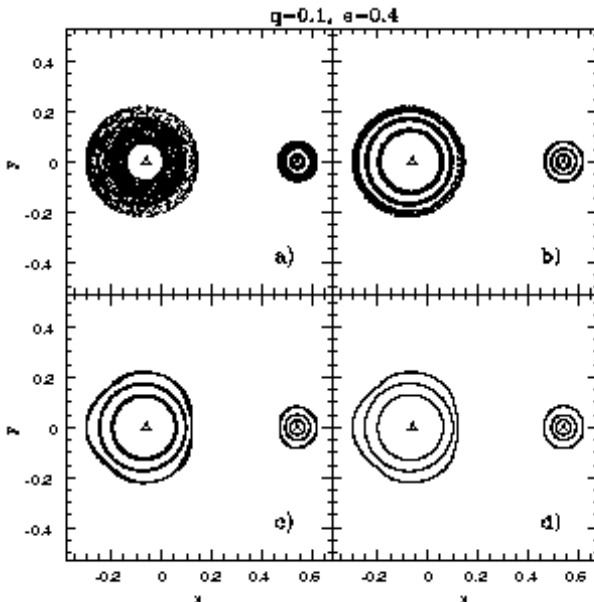


Figure 1. Searching for invariant circumstellar loops: successive positions at periastron of particles launched normally from the x -axis. In panels a) to d), the launch speeds approach those for stable loops, and the dispersion of the iterates decreases until the loop is found.

3 TEST: APPLICATION TO THE CIRCULAR BINARY CASE

In the limit that the binary's eccentricity goes to zero, the invariant loops should be exactly the closed circumstellar and circumbinary orbits (periodic orbits) for the circular system. We computed several orbits for cases with different mass ratios, to compare with other theoretical work.

We took arbitrary points of several computed loops as initial conditions to calculate the orbit in the non-inertial reference frame, corotating with the line that joins the stars. The resultant orbits indeed close on themselves, showing that for the circular binary, invariant loops are none other than the familiar periodic orbits.

In Figure 2 we show the invariant circumstellar loops found for a circular binary. The Jacobi constant is conserved within 10^{-9} . In the top panel are plotted the non-intersecting circumstellar loops, which could be populated by gas particles. In the bottom panel of this Figure we show an example of the intersecting loops that start mostly when the disks loops approach to the Roche lobe. These kind of loops, although stable, can not be populated by gas particles due to the intersection with the inner disk loops which would induce shocks dissipating first the less attached gas particles settle down in the intersecting loops. The dotted circles (aimed with straight arrows) represent a good fit to the radius of the Roche lobe as calculated by the analytic approximation by Eggleton (1983). For star i , the Roche radius R_i is given by

$$\frac{R_i}{a} \approx \frac{R_i(\text{Egg})}{a} = \frac{0.49q_i^{2/3}}{0.6q_i^{2/3} + \ln(1 + q_i^{1/3})}, \quad \text{where} \quad (4)$$

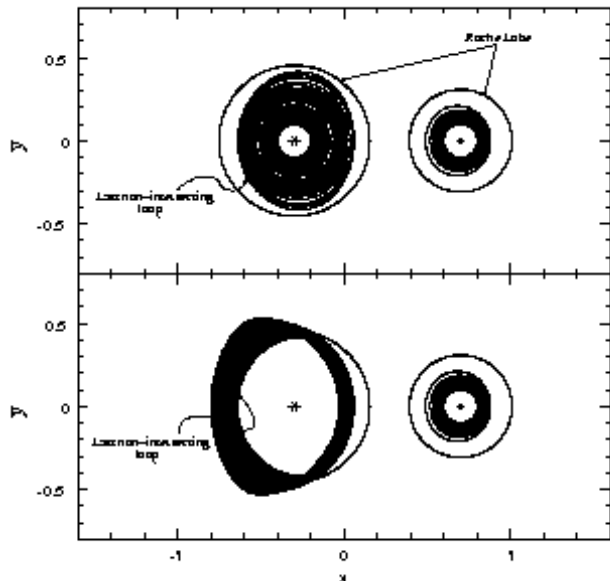


Figure 2. Points on the circumstellar invariant loops for the circular orbit, for a mass ratio $q=0.2$. Top panel: loops are plotted up to the position of the last non-intersecting loop (that defines the circumstellar gaseous disk). Bottom panel: loops are plotted starting from the last non-intersecting loop until the last loop found.

$$q_1 = m_1/m_2 = \frac{1-q}{q} \text{ and } q_2 = m_2/m_1 = \frac{q}{1-q}. \quad (5)$$

Note that the circumstellar periodic orbits are not circular, but are elongated perpendicular to the line joining the stars. Orbits very close to the Roche lobe change their shape dramatically crossing in some cases this frontier (e.g. circumpriary disk with $q = 0.4$) and producing intersections with the inner orbits. In an eccentric binary, the circumstellar disks tend to be also elongated in the same sense. In high eccentricity cases ($e > 0.4$), disks are nearly circular.

Using our method to search for invariant loops, we have computed the limiting radii of circumstellar and circumbinary disks for mass ratios q ranging from the Jupiter-Sun system ($q = 0.001$) to the equal-mass case $q = 0.5$. The limiting radii are selected as the loops overlap or when no more loops are found (the more common case when $e > 0$). In Figure 3, we present the disk sizes at periastron as a function of the mass fraction. For our limiting loops, we measured the disk extent in both directions along the x -axis joining the two stars. The nearly-vertical continuous lines marked at the top with L_1 , L_2 , L_3 are the Lagrange points. The circumstellar disks are confined within the Lagrange points, while the circumbinary disk is approximately centered on the origin, the mass center of the binary. The filled squares are the limiting radii found by Rudak & Paczyński (1981), who approximate the gas streamlines in pressureless accretion disks by non-intersecting simple periodic orbits. They compute in this way several disk sizes allowed by this potential. The results of our computations for disk sizes in the circular case are in very good agreement.

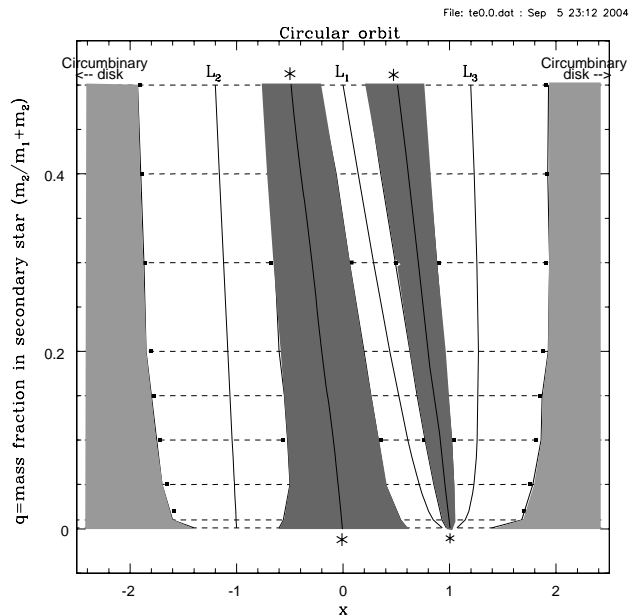


Figure 3. Shaded regions show the radii accessible to the circumstellar and the circumbinary disks as a function of the mass fraction, $q = m_2/(m_1 + m_2)$. The Lagrange points L_1 , L_2 , and L_3 are indicated, and the position of the stars is shown by near-vertical lines with a star at the top and bottom of each one. The horizontal lines show the actual mass fractions where the computations were done. With filled squares we mark for comparison some examples of the calculated radii from Rudak & Paczyński (1981).

4 THE GENERAL CASE: ECCENTRIC BINARIES

Unlike the zero eccentricity case, where particles see a simple time-steady potential, we now have a variation of the potential in time; in this manner particles will see a changing situation in any rotating reference frame. The phase space increases its dimensionality including now time as a canonical variable.

In the same manner as for the circular case, we have constructed figures showing disk sizes for eccentricities up to $e = 0.9$, for a given mass ratio q . In Figure 4 we show the regions accessible to circumstellar or circumbinary disks for a binary with a fixed mass ratio of $q = 0.1$ as the eccentricity grows. L_1 , L_2 , and L_3 are the Lagrangian points in the pericenter of the system multiplied by $(1 - e)$. The circumstellar disks become rapidly smaller as the binary grows more eccentric, while the circumbinary disk recedes. Additionally, in Table 1, we present the averaged radii of the circumstellar disks. In Table 2 we compare the averaged radius of the circumsecondary and circumpriary disks, respectively, with the Lagrangian radius computed at the pericenter multiplied by $(1 - e)$. For all mass ratios and $e \leq 0.8$, the size of the disk around the secondary star is well predicted as 0.4 ± 0.03 of the Lagrange radius times $(1 - e)$.

We have fitted a power law in both e and q to the calculated radii, for eccentricities in the range $[0.00, 0.9]$, and q in the range $[0.01, 0.99]$, obtaining the following relation for the size of the circumstellar disks:

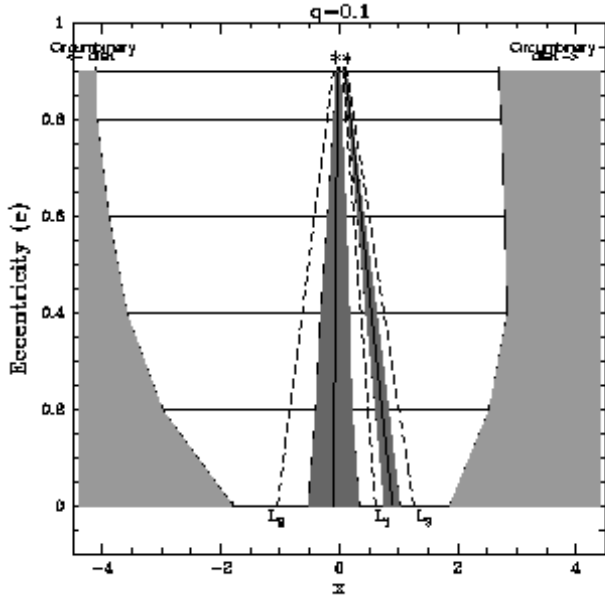


Figure 4. Similar to figure 3 (disks radii are computed at periastron) but with orbital eccentricity as ordinate for the case $q=0.1$. The position of the stars is shown by near-vertical lines with a star at the top of each one. The horizontal lines show the actual eccentricities where the computations were done. The dashed lines marked as L_1 , L_2 , and L_3 are the Lagrangian points for the circular binary, multiplied by $(1 - e)$.

$$R_i \approx R_{i,\text{Egg}} \times 0.733 (1 - e)^{1.20} q^{0.07} R_2, \quad (6)$$

where $R_{i,\text{Egg}}$ is Eggleton's estimate for the Roche Lobe average radius (equation 5). In Table 3 we have calculated the ratio between this quantity and the actual radii of the circumstellar disks computed; our formula is accurate to $\pm 6.5\%$.

In Table 4 we show the left and right radii of the circumbinary disk measured from the center of mass. A change in the mass fraction leaves the size and shape of the circumbinary disk almost unaffected. On the other hand, a slight increase in the eccentricity will result in a noticeable change as can be appreciated from Figure 4; The circumbinary disk is now off-center with respect to the center of mass; it almost preserves a constant distance from the closest approach of either star: see figures 5 and 6.

We have calculated the approximate position of the closest resonances at the edge of the circumstellar and circumbinary disks in all the computed cases presented. For the circular case, for mass ratios $q \geq 0.01$ all disks finish approximately at their 1:3 resonance. For an extreme mass ratio, as with the Sun-Jupiter case, the circumbinary and circumprimary disks can extend further, to the 1:2 resonance. As the eccentricity increases, the disk is truncated at successively higher order resonances. For $e \approx 0.2$ the closest resonances to the end of the circumstellar disks are 1:5 or 1:6. For a higher eccentricity ($e > 0.6$) the closest resonances are of even higher order (1:8 to 1:20). For the circumbinary disk at eccentricities, $e \geq 0.1$, the closest resonances to the inner boundary are 1:4 or 1:5.

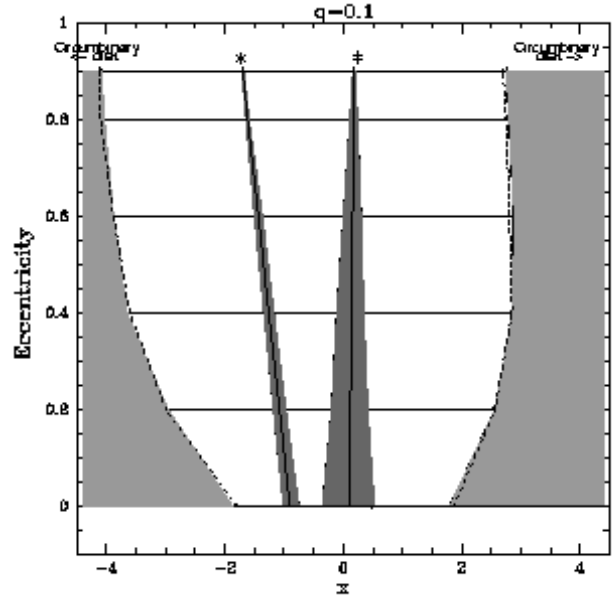


Figure 5. As Figure 4, but at apastron: boundaries of the circumstellar disks and the inner edge of the circumbinary disk, for mass ratio $q = 0.1$, as a function of eccentricity e . Dashed lines indicate the inner boundary of the circumbinary disk in Figure 4: showing that the position of this disk changes little with binary phase.

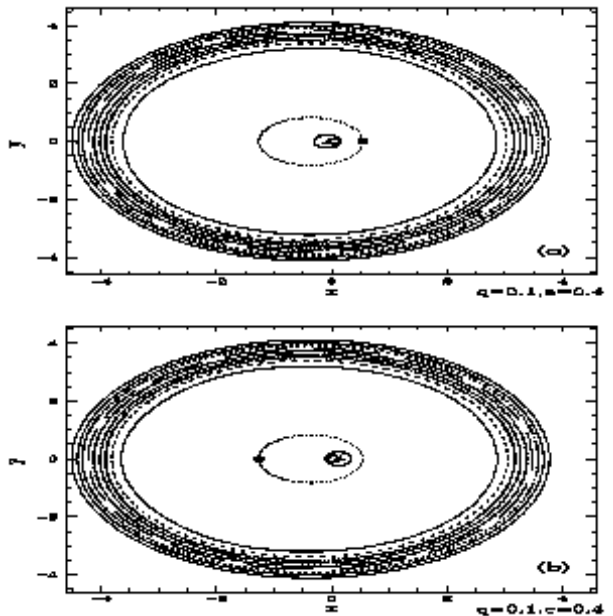


Figure 6. Circumbinary disk calculated at the binary pericenter (a), and at the apocenter (b), for the case $q = 0.1$, $e = 0.4$. Dotted curves in the center show the stars trajectories; and small curves surrounding the stars (which are pointed by triangles) show the extent of circumstellar disks.

Table 1. Averaged radius of disk around star 2 (secondary for $q < 0.5$, primary for $q > 0.5$) in units of the semimajor axis, a . All radii are measured from the outermost loop at the binary periastron.

m_2 / e	0.0	0.2	0.4	0.6	0.8
0.1	0.125	0.100	0.079	0.049	0.019
0.2	0.162	0.130	0.098	0.048	0.029
0.3	0.195	0.165	0.097	0.067	0.028
0.4	0.228	0.195	0.125	0.083	0.033
0.5	0.257	0.213	0.147	0.097	0.037
0.6	0.317	0.228	0.153	0.093	0.047
0.7	0.350	0.225	0.171	0.109	0.037
0.8	0.387	0.260	0.187	0.126	0.049
0.9	0.426	0.297	0.231	0.141	0.064

Table 2. Averaged radius of the disk around star 2 (secondary for $q < 0.5$, primary for $q > 0.5$) compared with Lagrangian radii calculated at the pericenter: $\frac{1}{2}(L1 - L)(1 - e)$, where $L = L3$ for $q = [0.1, 0.5]$, and $L = L2$ for $q = [0.5, 0.9]$.

m_2 / e	0.0	0.2	0.4	0.6	0.8
0.1	0.38	0.39	0.40	0.38	0.30
0.2	0.39	0.39	0.39	0.29	0.34
0.3	0.40	0.42	0.33	0.34	0.29
0.4	0.42	0.44	0.38	0.38	0.30
0.5	0.43	0.44	0.41	0.40	0.31
0.6	0.49	0.44	0.39	0.36	0.36
0.7	0.50	0.40	0.40	0.39	0.26
0.8	0.51	0.43	0.41	0.41	0.33
0.9	0.52	0.45	0.47	0.43	0.39

Table 3. Same as Table 2 but the disk radius is compared with the radius R_i obtained from equation 6.

m_2 / e	0.0	0.2	0.4	0.6	0.8
0.1	0.93	0.98	1.09	1.10	0.98
0.2	0.91	0.95	1.02	0.81	1.12
0.3	0.92	1.01	0.84	0.94	0.91
0.4	0.93	1.04	0.94	1.02	0.93
0.5	0.93	1.00	0.98	1.05	0.92
0.6	1.01	0.95	0.90	0.89	1.04
0.7	0.99	0.83	0.89	0.93	0.72
0.8	0.96	0.84	0.85	0.93	0.83
0.9	0.87	0.80	0.88	0.87	0.91

Table 4. Coordinates where the inner edge of the circumbinary disk crosses the x axis, in units of the semimajor axis, a

m_2 / e	0.0	0.2	0.4	0.6	0.8
0.1	-1.80,1.87	-3.00,2.54	-3.60,2.85	-3.90,2.80	-4.10,2.75
0.2	-2.00,2.04	-3.00,2.56	-3.70,3.05	-3.90,2.86	-4.00,2.84
0.3	-1.90,1.94	-3.20,2.98	-3.60,3.12	-3.80,3.16	-4.00,3.33
0.4	-1.90,1.92	-3.10,2.98	-3.50,3.27	-3.70,3.40	-3.70,3.30
0.5	-2.00,2.00	-2.70,2.70	-2.90,2.90	-3.40,3.40	-3.40,3.40

5 MORPHOLOGY AND TEMPORAL EVOLUTION

Although the disks were calculated when the stars are at their pericenter, they can be followed to any other phases of the binary. In Figure 7, we see that the morphology of the disks changes slightly for different phases. The maximum change in radius is generally about 5% of the radius measured at pericenter, increasing or decreasing with no preference for any specific phase.

The loops that form the circumbinary disks are nearly circular close to the corresponding star, up to about 80% of the outer radius; there the shape can change abruptly to become more elliptical. This is more pronounced when the binary is *less* eccentric, because the disk then extends further in radius. The loops are also slightly off-centered. We can measure this by sampling the distance s of each circumbinary loop from the star at N points equally spaced

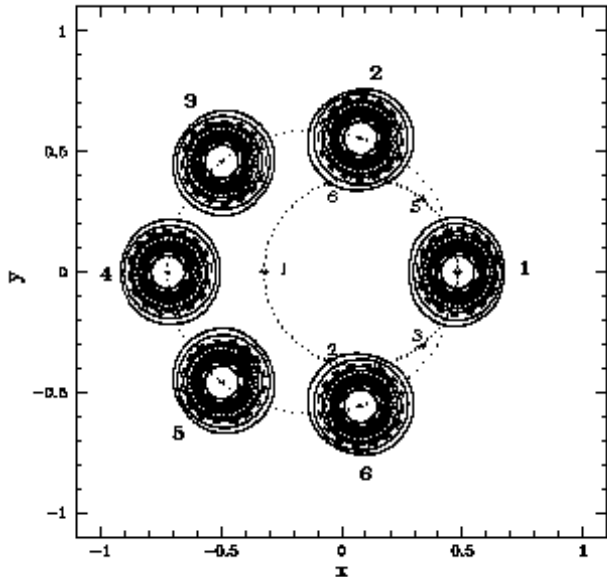


Figure 7. The circumsecondary disk at 6 different phases of the binary, for the case $q = 0.4$, $e = 0.2$. Dotted lines show the orbits of both primary and secondary stars; asterisks show the positions at corresponding times.

in azimuthal angle ϕ around it, and computing the Fourier coefficients

$$A_k = \frac{1}{N} \sum_{i=0}^N s(\phi) \cos(k\phi), \quad (7)$$

$$B_k = \frac{1}{N} \sum_{i=0}^N s(\phi) \sin(k\phi). \quad (8)$$

The lopsidedness of the disks at the binary pericenter is measured by computing $\sqrt{A_1^2 + B_1^2}/r_{peri}$, (and the ellipticity by $\sqrt{A_2^2 + B_2^2}/r_{peri}$), where r_{peri} is the azimuthally-averaged radius of the circumstellar loop. We find that the maximum lopsidedness of the outermost circumstellar loops at pericenter is 5%. The lopsidedness changes by less than 1% with the binary phase.

For the circumstellar disks we measure the maximum ellipticity at pericenter by computing $ell = 1 - b/a$, the ratio of the major axis, which is always perpendicular to the line that joins the stars, to the minor axis which lies along the line joining the stars. The ellipticity of the outermost circumstellar loop at the pericenter is higher in the binaries with lower eccentricities ($e < 0.4$), since these disks extend much further inward in radius (see Figure 5); it is generally in the range $0.08 < ell < 0.2$. For the circumbinary disks the maximum ellipticity of the inner edge is generally reached when the stars are at the apocenter and is $ell \approx 0.05$. The maximum change in the ellipticity for the circumbinary disks with phase is 5% of the ellipticity at the pericenter.

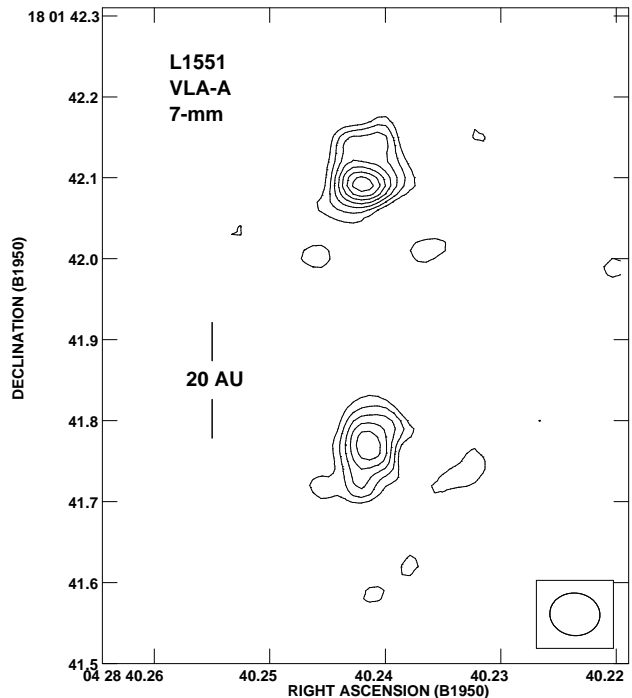


Figure 8. Cleaned, natural-weight VLA map of the L1551 IRS5 region at 7-mm. Figure 1 of Rodríguez et al. (1998). The emission shown in this map is interpreted to arise from two compact protoplanetary structures forming a gravitationally-bound binary system.

6 APPLICATION TO OBSERVATIONS

Observational parameters of only a very few binaries with accretion or proto-planetary disks are known. We have chosen as an application a couple of well-known examples of these kind of systems for which some important parameters (like the size of the observed disks or the orbital parameters) are known; the first is related to accretion (L1551), and the second to protoplanetary disks (α Centauri).

In this case, for example, if the disks radii and the distance between the stars are known, we can approach the orbital parameters and mass ratios. On the other hand, if the orbital parameters, like eccentricity, and semimajor axis of the binary orbit are known, the potential sizes of the circumstellar and circumbinary disks can be readily calculated.

6.1 Circumstellar disks around the L1551 binary

Rodríguez et al. (1998, 2003) report interferometric observations at 7 mm showing hot dust in the core of the star-forming region L1551, a molecular cloud in Taurus. In the resolved core of L1551 are two distinct disks with a separation of 45 AU that appear to be circumstellar disks associated with a binary system (Figure 8). With accretion disk models they find that best fits to the data are obtained for disks with semi-major axes of about 10 AU and total masses of approximately $0.05 M_{\odot}$, enough to form protoplanetary disks. The

disks are apparently elongated towards each other. Since the circumstellar loops tend to be elongated in the perpendicular sense, this suggests that the binary orbit is tilted an angle of approximately 60° to our line of sight, as models of the system and its jets indicate (Rodríguez et al. 2003; Osorio et al. 2003). The stars now lie close to the line of nodes of the orbit so the observed separation is close to the true separation (Rodríguez et al. 2003). Millimetre-wave observations suggest the system is embedded in an elongated structure of dust and gas with scales of 100-400 AU (Lay et al. 1994; Keene & Mason 1990). This structure may correspond to a circumbinary ring or disk (Looney et al. 1997), that would probably be providing enough material to fill the circumstellar disks.

Proper motions do not give clear information about the orbit, but we can use the disk sizes to set bounds on the eccentricity and the mass ratio of the system. For any fixed eccentricity, Table 5 shows that for a mass ratio $q = 0.4$, or $m_1 : m_2 = 3 : 2$, the circumsecondary disk should be roughly 60% smaller than the circumpriary disk. Since we see two nearly equal disks, this implies $0.4 \leq q \leq 0.5$ for this system. If we assume that is a circular orbit, the circumstellar disks could both extend to 13.5 AU if the stellar masses are equal, or 9.5 and 15.3 AU for circumsecondary and circumpriary disks respectively, if $q = 0.4$. The circumbinary disk gap would then end about 90 AU from the center of mass of the system. The measured disks are only approximately 10 AU in radius, which might be probably due simply to the fact that the emission weakens, make it difficult to detect, however we have also explored the possibility that the reduced size of the disks is due to the fact that the binary orbit is slightly eccentric, in this manner we have constructed a range of possibilities for this system. For $e > 0.2$, Table 5 shows that the disks should be truncated short of their observed extent of 10 AU ; so we conclude that the eccentricity of the system is in the interval $e = [0, 0.2]$. The extreme case with $q = 0.4$, and $e = 0.2$, would produce very different disk sizes ($r_{prim}/r_{sec} \sim 1/2$), so we discard this possibility also. Thus the system parameters are constrained approximately by $(0.5 - q) + 0.5e \leq 0.1$.

6.2 Zones for Planets around Alpha Centauri

As one of the alternatives to form planets in accretion disks arised the “planetesimal theory”: planets are formed in circumstellar dust disks, where colliding dust grains accrete into planetesimals approximately of 1-10 km of diameter (Safronov 1969; Lissauer 1993). As the sizes of particles increase and gravitational attraction becomes more important, the cross-section for accretion also increases, as more and more particles collide. This effect, combined with dynamical friction, leads to “runaway growth”: large bodies accrete more efficiently than small bodies, becoming planetary embryos that increase their masses through collisions until most of the material is accreted or dispersed by these new protoplanets (Greenberg et al. 1978; Wetherhill & Stuart 1989). Assuming that planets are initially formed in accretion disks, invariant loops can give us also a good idea of what possibilities a binary system has to harbor stable planets, and the maximum radius of a protoplanetary disk that can give rise to them.

α Centauri is composed of a binary star consisting on

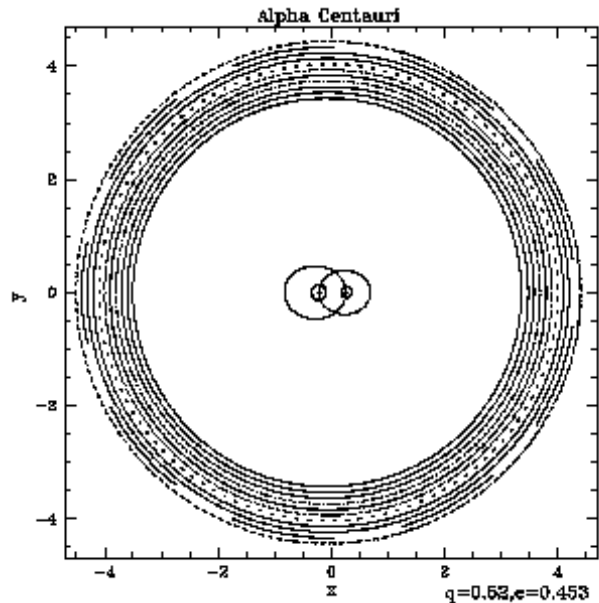


Figure 9. Circumbinary disk constructed with invariant loops applied to the case of α Centauri. Ellipses at the center mark the stellar trajectories. Smaller curves around the two three-pointed stars mark the limit of the circumstellar disks.

a G2 star with $1.1 M_\odot$ (α Centauri A) and a K1 star with $0.91 M_\odot$ (α Centauri B) and a third component (α Centauri C or Proxima Centauri), which is thought to orbit this pair but at a very large distance (12,000 AU). The binary system has an eccentricity of 0.52 and a semimajor axis of 23.4 AU (See 1893, Heintz 1982).

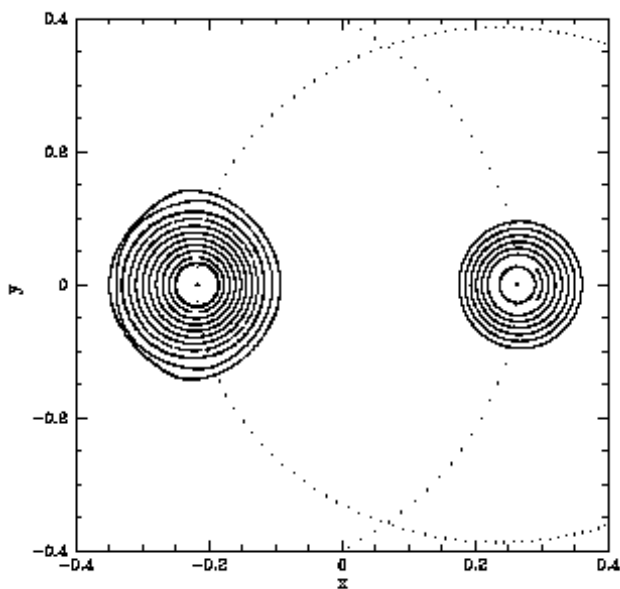
This system and the stability of planets around them has been extensively studied. Wiegert & Holman (1997) used direct numerical integration to find that planets orbiting prograde in the plane of α Centauri A and B within 3 AU of either star can be stable for several million years, as can planets in circumbinary orbit more than 70 AU from the center of mass of the system. Marziari & Scholl (2000) studied the evolution of planetesimals perturbed by gas drag in a disk in the plane of the binary system, finding that planetesimals are able to accrete one another within 2 AU of α Cen A. Quintana et al. (2002) follow the growth of planetary embryos under the gravitational forces of the binary system using a symplectic N-body accretion algorithm, finding stable planets in prograde orbits up to 2.5 AU from either star, and showing how for high inclinations of the orbits, with respect to the plane of the binary, they become unstable.

Circumbinary and circumstellar disks constructed with invariant loops applied to the case of α Centauri are presented in Figures 9 and 10. We calculated a size of 3 AU for the circumstellar disk (or potential protoplanetary disk) around α Centauri A, and 2.3 AU for α Centauri B. The circumbinary gap, measured from the center of mass, should extend to 80 AU .

In Figure 11 we show the evolution of the circumpriary disk (α Centauri A) with the phase. The disk changes its shape and slightly its size as it evolves in time. While it is unlikely that such small changes in shape could be ob-

Table 5. Binary parameters for possible L1551 IRS5 models, and the implied sizes of the circumstellar disks

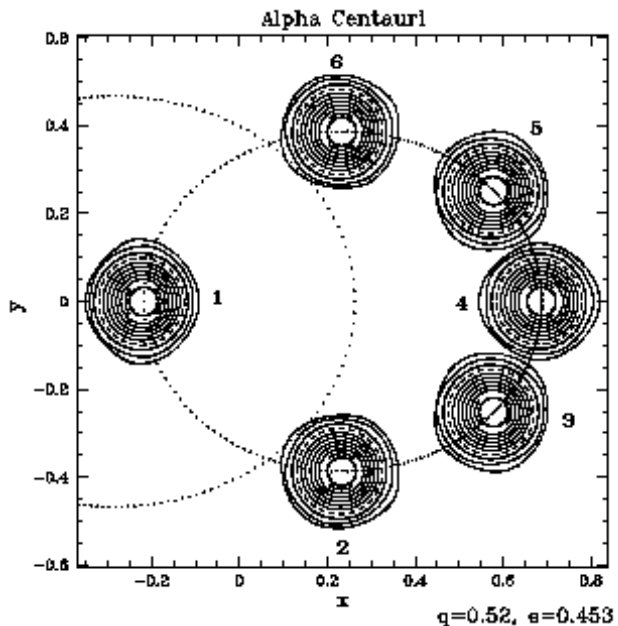
q, e	present phase	a (AU)	r_{sec}	r_{prim}	r_{CB}
$q = 0.5, e = 0.0$		45	13.5	13.5	88
$q = 0.4, e = 0.0$		45	9.5	15.3	86
$q = 0.5, e = 0.2$	peri	56	11.2	11.2	152
$q = 0.5, e = 0.2$	apo	37.5	7.5	7.5	101
$q = 0.4, e = 0.2$	peri	56	14.6	7.3	157
$q = 0.4, e = 0.2$	apo	37.5	9.75	4.9	105

**Figure 10.** A zoom of the circumstellar disks shown in Figure 9.

served directly, the crowding of orbits at phases 1, 2, and 5 are likely to lead to increased heating and inflow when the disk contains gas.

7 CONCLUSIONS

With the concept of *invariant loop*, we have extended the possibilities for orbital studies in accretion or protoplanetary disks of binary stellar systems, with no restriction on the mass ratio (q) or eccentricity (e) of the binary. In this manner the method represents an extension to the periodic-orbit analysis in the well-known circular case. Sweeping the parameter space, we are able to address the limits and possibilities for gaseous circumstellar and circumbinary disks from the point of view of the “pure” potential exerted by the binary. In the case of accretion disks, this approximation would closely represent the low viscosity regime of the gas. Although the studies presented in this work were restricted to the plane of the disks, this technique can also be applied to orbits out of the plane of the binary orbit. Compared with high-resolution hydrodynamic simulations the method is computationally cheap and fast.

**Figure 11.** Six phases of the α Centauri circumpriary disk constructed with invariant loops. Dotted curves show stellar trajectories. Numbers show the ordered phases, as in Figure 7.

We find that the size of the circumstellar and circumbinary disks depends strongly on the eccentricity. The average radius of the circumstellar disks is approximately 40% of the Lagrangian radius calculated at the pericenter of the binary orbit. Equation 6 provides a more accurate analytic approximation to the disk size.

The inner radius of the circumbinary disks (the *gap* radius) is practically independent of the mass ratio. For the circular binary, the circumbinary disk ends close to the 1:3 resonance for non-extreme mass ratios ($q \geq 0.01$). For higher eccentricities, the inner edges of the circumbinary disks appear to be truncated close to higher order resonances (1:4, to 1:6). Even a slight increase in eccentricity for a given mass ratio will cause the gap to grow to much larger radii. The inner edge of a circumbinary disk is not centered at the center of mass; instead particles in the disks appear to pass at near-equal distances from the apocenter positions of the two stars.

In the temporal evolution, the circumbinary disks show almost no change with binary phase, while the circumstellar disks change their shape and size only slightly. The average

radius changes by only 5% at different phases of the binary. The largest or smallest radius can be reached at any phase, i.e., there is no preference for larger radii at any specific phase.

Near the outer edge, the shape of the disks become less circular in general and slightly off-centered, by up to 5%. The change of lopsidedness with the phase is less than 1% of the lopsidedness measured at the pericenter of the binary.

For the circumstellar disks the maximum ellipticity is in most cases reached at pericenter, where the semimajor axes of the circumstellar disks are perpendicular to the line that joins the stars. The ellipticity at the pericenter is higher in the cases with lower eccentricities ($e < 0.4$) and it is generally below $ell \approx 0.2$. For larger eccentricities the ellipticity of the circumstellar disks is $ell < 0.08$. The maximum change of ellipticity with time is 7% of the ellipticity measured at the pericenter of the binaries.

For the circumbinary disks the maximum ellipticity is generally reached when the stars are at the apocenter and is $ell \approx 0.05$. The maximum change in the ellipticity for the circumbinary disks with phase is 5% of the ellipticity at the pericenter.

As an application to observations we selected two specific objects: L1551-IR5 and α Centauri. Assuming that the line that joins the stars rests approximately in the plane of the sky, the eccentricity of the system in L1551-IR5 is $e \leq 0.2$ and the mass ratio is $q \approx 0.5$. The circumbinary inner edge disk should lie approximately at 90 AU if $e = 0$, and in the interval 100-150 AU for the extreme case $e = 0.2$. In the case of α Centauri, we calculated the zones for planets around each star and around the binary. We find that for α Cen A, the last stable loop reaches 3 AU, while for α Cen B it is at 2.3 AU. Beyond the gap, the innermost invariant loops start at a distance of 80 AU from the center of mass.

Every day, disks are being discovered in more binary (and multiple) stellar systems. Theoretical studies of these systems can help to restrict their geometrical characteristics, and may also help to constrain some other unknown physical characteristics like viscosity.

ACKNOWLEDGMENTS

We thank Luis Felipe Rodríguez for supplying Figure 8. L. S. and B. P. thank NASA and the Space Telescope Science Institute for support through grant HST-AR-09522.01-A. L. A. is grateful to the Department of Astronomy of the University of Wisconsin-Madison for a fruitful sabbatical stay where this work got started. He also acknowledges support from DGAPA/UNAM through grant IN113403. B. P. thanks Mexico's CONACyT for a postdoctoral fellowship, and NASA for support through grant NAG5-10823.

REFERENCES

- Abt, H. A. 1977, *Sci.Am.*, 236, 96
 Arnold, V.I. 1984, *Mathematical Methods of Classical Mechanics*, (Springer-Verlag)
 Artymowicz, P., & Lubow, S. H. 1994, 421, 651
 Bate, M. R., 1997, *MNRAS*, 285, 16
 Bate, M. R., & Bonnell, I. A. 1997, *MNRAS*, 285, 33
 Bate, M. R., & Bonnell, I. A., Bromm, V. 2002, *MNRAS*, 336, 705
 Bonnell, I., & Bastien, P. 1992, *IAU Colloquium* 135, 32, 206
 Butler, R. P., Marcy, G. W., Williams, E., Hauser, H., & Shirts, P. 1997, *ApJ*, 474, 115
 Cochran, W. D., Hatzes, A. P., Butler, R. P., & Marcy, G. W. 1997, *ApJ*, 483, 457
 David, E, Quintana, E. V., Fatuzzo, M., Adams, F. C. 2003, *PASP*, 115, 825
 Duquennoy, A., & Mayor, M. 1991, *A&A*, 248, 485
 Eggleton, P. P. 1983, *ApJ*, 268, 368
 Fischer, D. A., & Marcy, G. W. 1992, *ApJ*, 396, 178
 Foulkes, S. B., Haswell, C. A., Murray, J. R., Rolfe, D. J. 2004, *MNRAS*, 349, 1179
 Ghez, A. M., Neugebauer, G., & Matthews, K. 1993, *A. J.*, 106, 2005
 Greenberg, R., Hartmann, W. K., Chapman, C. R., Wacker, J. F. 1978, *Icarus*, 35, 1
 Goldstein, H. 1922, *Classical Mechanics*, (3d ed.; Addison Wesley)
 Guerrero, J., García-Berro, E., Isern, J. 2004, *A&A*, 413, 257
 eintz, W. D. 1982, *Obs*, 102, 42
 Jensen, E. L. N., Mathieu, R. D., Donar, A. X., Dullighan, A. 2004, *ApJ*, 600, 789
 Kastner, J. H., Huenemoerder, D. P., Schulz, N. S., Canizares, C. R., Li, J., Weintraub, D. A. 2004, *ApJ*, 605, 49
 Keene, J., Masson, C. R. 1990, *ApJ*, 355, 635
 Kortenkamp, S. J., Wetherill, G. W., & Inaba, S. 2001, *Science*, 293, 1127
 Lanzafame, G. 2003, *A&A*, 403, 593
 Lay, O. P., Carlstrom, J. E., Hills, R. E., Phillips, T. G. 1994, *ApJ*, 434, 75
 Leinert, Ch., Zinnecker, H., Weitzel, N., Christou, J., Ridgway, S. T., Jameson, R., Haas, M., & Lenzen, R. 1993, *A&A*, 278, 129
 Lichtenberg, A.J., & Lieberman, M.A. 1992, *Regular and Chaotic Dynamics*, (2d ed.; New York: Springer)
 Lissauer, J. J. 1993, *ARA&A*, 31, 129
 Liu, M. C., Najita, J., Tokunaga, A. T. 2003, *ApJ*, 585, 372
 Looney, L. W., Mundy, L. G., Welch, W. J. 1997, *ApJ*, 484, 157
 Lubow, S. H., & Shu, F. H. 1975, *ApJ*, 198, 383
 Maciejewski, W., Sparke L. S. 1997, *ApJL*, 484, 117
 Masciadri, E., Raga, A. C. 2002, *ApJ*, 568, 733
 Mathieu, R. D., Walter, F. M. & Myers, P. C. 1989, *AJ*, 98, 987
 Mathieu, R. D., Ghez, A. M., Jensen, E. L. N., & Simon, M. 2000, in *Protostar and Planets IV*, ed. V. Mannings, A. P. Boss, & S. S. Russell (Tucson: Univ. Arizona Press) 731
 Nielbock, M., Chini, R., Müller, S. A. H. 2003, *A&A*, 408, 245
 Osorio, M., D'Alessio, P.; Muzerolle, J., Calvet, N., Hartmann, L. 2003, *ApJ*, 586, 1148
 Papaloizou, J., & Pringle, J. E. 1977, 181, 441
 Paczyński, B. 1977, *ApJ*, 216, 822
 Pogodin, M. A., Miroshnichenko, A. S., Tarasov, A. E., Mitskevich, M. P., Chountonov, G. A., Klochkova, V. G.,

- Yushkin, M. V., Manset, N., Bjorkman, K. S., Morrison, N. D., Wisniewski, J. P. 2004, *A&A*, 417, 715
- Quintana, E. V., Lissauer, J. J., Chambers, J. E., Duncan, M. J. 2002, *ApJ*, 576, 982
- Reipurth, B., & Zinnecker, H. 1993, *A&A*, 278, 81
- Rodríguez, L. F., D'alessio, P., Wilner, D. J., Jo, P. T. P., Torrelles, J. M., Curiel, S., Gómez, Y., Lizano, S., Pedlars, A., Cantó, J., & Raga, A. C. 1998, *Nature*, 395, 355
- Rodríguez, L. F., Curiel, S., Cantó, J., Loinard, L., Raga, A. C., Torrelles, J. M. 2003, *ApJL*, 583, 330
- Rudak, B., Paczynski, B. 1981, *Acta Astron*, 31, 13
- Safronov, V. S. 1969, *Evolution of the Protoplanetary Cloud and Formation of the Earth and the Planets* (Moscow: Nauka)
- Schaefer, G. H., Simon, M., Nelan, E., Holfeltz, S. T. 2003, *AJ*, 126, 1971
- See, T. J. J. 1893, *MNRAS*, 54, 102
- Simon, M., Ghez, A. M., Leinert, Ch., Cassar, L., Chen, W. P., Howell, R. R., Jameson, R. F., Matthews, K., Neugebauer, G., & Richichi, A. 1995, *ApJ*, 443, 625
- Wetherhill, G. W., & Stuart, G. R. 1989, *Icarus*, 77, 330